CSIRO Publishing

Publications of the Astronomical Society of Australia

VOLUME 18, 2001

An international journal of astronomy and astrophysics

For editorial enquiries and manuscripts, please contact:
The Editor, PASA,
ATNF, CSIRO,
PO Box 76,
Epping, NSW 1710, Australia
Telephone: +61 2 9372 4590
Fax: +61 2 9372 4310
Email: Michelle.Storey@atnf.csiro.au

For general enquiries and subscriptions, please contact:
CSIRO Publishing
PO Box 1139 (150 Oxford St)
Collingwood, Vic. 3066, Australia
Telephone: +61 3 9662 7666
Fax: +61 3 9662 7555
Email: pasa@publish.csiro.au

Published by CSIRO Publishing
for the Astronomical Society of Australia

www.publish.csiro.au/journals/pasa

https://doi.org/10.1071/AS01022 Published online by Cambridge University Press

Publ. Astron. Soc. Aust., 2001, 18, 201–206

Cosmological Parameter Survey Using the Gravitational Lensing Method

Premana W. Premadi[1], Hugo Martel[2], Richard Matzner[3] and Toshifumi Futamase[4]

[1]Department of Astronomy and Bosscha Observatory, Institut Teknologi Bandung, Indonesia
premadi@as.itb.ac.id
[2]Department of Astronomy, University of Texas, Austin, USA
hugo@simplicio.as.utexas.edu
[3]Center for Relativity, Department of Physics, University of Texas, Austin, USA
richard@ricci.ph.utexas.edu
[4]Astronomical Institute, Tohoku University, Sendai, Japan
tof@astr.tohoku.ac.jp

Received 2001 January 21, accepted 2001 March 9

Abstract: Using a multiple-lens plane algorithm, we study light propagation in inhomogeneous universes for 43 different *COBE*-normalized Cold Dark Matter models, with various values of the density parameter Ω_0, cosmological constant λ_0, Hubble constant H_0, and rms density fluctuation σ_8. We performed a total of 3798 experiments, each experiment consisting of propagating a square beam of angular size $21.9'' \times 21.9''$ composed of 116 281 light rays from the observer up to redshift $z = 3$. These experiments provide statistics of the magnification, shear, and multiple imaging of distant sources. The results of these experiments might be compared with observations, and eventually help constrain the possible values of the cosmological parameters. Additionally, they provide insight into the gravitational lensing process and its complex relationship with the various cosmological parameters.

Keywords: cosmology: large-scale structure — gravitational lensing

1 Introduction

The evolution of a homogeneous, isotropic, expanding universe comprised of nonrelativistic matter can be described in terms of three parameters: the Hubble constant H_0, the density parameter Ω_0, and the cosmological constant λ_0. The large-scale structure of the universe, galaxies, clusters, and voids, represents the deviations from this overall homogeneity and isotropy. These structures originate from primordial fluctuations that grow with time as a result of gravitational instability. Determining the value of the cosmological parameters, and the correct model of large-scale structure formation, is the most important challenge of observational and physical cosmology.

In recent years, gravitational lenses have been used to estimate or put limits on the values of the cosmological parameters (amongst others: Fukugita, Futamase & Kasai 1990; Turner 1990; Martínez-González, Sanz & Cayón 1997; Wambsganss et al. 1997; Kundić et al. 1997; Falco, Kochanek & Muñoz 1998; Chiba & Yoshii 1999; Barber et al. 2000). If the cosmological model has several free parameters, a full survey of the cosmological parameter space is required in order to determine or limit the values of all cosmological parameters *simultaneously*. We present a study of light propagation in inhomogeneous universes surveying the full 4-parameter phase-space formed by Ω_0, λ_0, H_0, and n, the slope of the primordial power spectrum.

2 The Ray-Tracing Experiments

To simulate light propagation in inhomogeneous universes, we use a newly developed version of the *Multiple Lens-Plane Algorithm* (Schneider, Ehlers & Falco 1992; Jaroszyński 1992; Martel, Premadi & Matzner 1998; Premadi, Martel & Matzner 1998). Our algorithm uses a P^3M code with 64^3 particles to simulate the formation and evolution of large-scale structure in the universe inside a computational volume of comoving size $L_{\rm box} = 128$ Mpc. The result is then used as the underlying distribution of dark matter in locating galaxies inside the computational volume by using an empirical Monte Carlo method. Each galaxy is modelled by a truncated, non-singular isothermal sphere. By combining the distribution of background matter simulated by the P^3M algorithm with the distribution and surface densities of galaxies, we effectively describe the surface density of the lens planes over eight orders of magnitude in length, from the size of the largest superclusters and voids, $\sim$100 Mpc, down to the core radii of the smallest galaxies, $\sim$1 pc.

We consider Tilted Cold Dark Matter models (TCDM), normalized to *COBE*. The power spectrum for this model is characterized by six independent parameters: Ω_0, $\Omega_{\rm B0}$ (the density parameter of the baryonic matter), λ_0, H_0, $T_{\rm CMB}$ (the temperature of the cosmic microwave background), and n. The normalization of the power spectrum is often described in terms of the rms density fluctuation σ_8 at a scale of $8\,h^{-1}$ Mpc. The value of σ_8 is a

10.1071/AS01022 1323-3580/01/020201$05.00

Table 1. Parameters of the 43 cosmological models, including, for each model, the independent parameters Ω_0, λ_0, H_0, and σ_8, and the dependent parameter n. H_0 is in units of km s^{-1} Mpc^{-1}

Ω_0	λ_0	H_0	σ_8	n	Ω_0	λ_0	H_0	σ_8	n
0.2	0.0	55	0.3	1.2187	0.5	0.5	65	0.8	0.7808
0.2	0.0	65	0.3	1.0966	0.5	0.5	65	1.0	0.8807
0.2	0.0	65	0.5	1.3188	0.5	0.5	75	0.8	0.7049
0.2	0.0	75	0.3	0.9993	0.5	0.5	75	1.0	0.8024
0.2	0.0	75	0.4	1.1228	0.7	0.0	65	0.9	0.8461
0.2	0.0	75	0.5	1.2190	0.7	0.0	65	1.1	0.9346
0.2	0.0	75	0.6	1.2979	0.7	0.0	75	0.9	0.7773
0.2	0.0	75	0.7	1.3648	0.7	0.0	75	1.1	0.8648
0.2	0.0	85	0.3	0.9191	0.7	0.3	65	0.9	0.7720
0.2	0.8	55	0.8	1.2057	0.7	0.3	65	1.1	0.8601
0.2	0.8	65	0.6	0.9326	0.7	0.3	75	0.9	0.7042
0.2	0.8	65	0.7	1.0062	0.7	0.3	75	1.1	0.7912
0.2	0.8	65	0.8	1.0702	1.0	0.0	55	1.0	0.8465
0.2	0.8	65	0.9	1.1269	1.0	0.0	65	0.9	0.7234
0.2	0.8	65	1.0	1.1568	1.0	0.0	65	1.0	0.7698
0.2	0.8	75	0.6	0.8273	1.0	0.0	65	1.1	0.8120
0.2	0.8	75	0.8	0.9629	1.0	0.0	65	1.2	0.8506
0.2	0.8	85	0.8	0.8749	1.0	0.0	65	1.3	0.8861
0.5	0.0	65	0.8	0.9457	1.0	0.0	75	1.0	0.7094
0.5	0.0	65	1.0	1.0439	1.0	0.0	75	1.2	0.7893
0.5	0.0	75	0.8	0.8686	1.0	0.0	85	1.0	0.6605
0.5	0.0	75	1.0	0.9656					

function of the six aforementioned parameters. We invert this relation, treating σ_8 as an independent parameter, and the tilt n as a dependent one. We also set $T_{\rm CMB} = 2.7$ K and $\Omega_{\rm B0} = 0.015\,{\rm h}^{-2}$. The independent parameters in this parameter space are therefore Ω_0, λ_0, H_0, and σ_8. We survey this parameter space by considering 43 different cosmological models. The values of the parameters are listed in Table 1. For each model, we performed from 50 to 200 ray-tracing experiments (depending on the statistical significance of the results) for a total of 3798 experiments. In each experiment, we compute the propagation of a beam consisting of $341^2 = 116\,281$ light rays forming a square lattice on the image plane. The size of the beam is $21.9'' \times 21.9''$, and the separation between rays is $21.9''/341 = 0.064''$. The beams are propagated from redshift $z = 0$ to $z \sim 3$ (sources at redshifts $z > 3$ would produce qualitatively similar results).

3 The Elements of Gravitational Lensing

Here we review the elements of gravitational lensing, in particular the dependence of these elements on the cosmological parameters. This will facilitate the interpretation of the results presented in the following section.

- The cosmological distances: The angular displacement caused by lensing depends on the angular diameter distances between the source and the observer, $D_{\rm S}$, the source and the lens, $D_{\rm LS}$, and the lens and the observer, $D_{\rm L}$. These distances depend on Ω_0, λ_0, and H_0, but not σ_8.
- The mean background density: The importance of lensing depends on the mean density of matter between the source and the observer, which is proportional to $\Omega_0 H_0^2$. Hence, the mean density depends on H_0 and Ω_0, but not λ_0 and σ_8.
- The large-scale structure: Most of the matter responsible for lensing is located at intermediate redshift z_L, half-way between the source and the observer. The rms density fluctuation $\sigma_{8,\rm L}$ at that redshift is given by $\sigma_{8,\rm L} \approx \sigma_8/\mathcal{L}(z_{\rm L}, 0)$, where $\mathcal{L}(z_{\rm L}, 0)$ is the linear growth factor between redshifts $z_{\rm L}$ and $z = 0$, which depends on Ω_0 and λ_0. Thus, $\sigma_{8,\rm L}$ depends on σ_8, Ω_0, and λ_0, but not H_0.

4 Results

4.1 The Magnification Distributions

Figure 1 shows the magnification distribution $P(\mu)$ for various models. The top left panel shows the effect of varying σ_8. As σ_8 increases, the peak of the distribution decreases, the low edge of the distribution moves to even lower values, but the right edge is hardly affected. The explanation is the following: a larger σ_8 implies that (1) the underdense regions are more underdense and the overdense regions are more overdense, and (2) the fraction of the universe occupied by underdense regions (the 'filling factor') increases while the fraction occupied by overdense regions decreases. In the case of demagnification, these two effects act in the same direction: as σ_8 increases, the beam is more likely to propagate through an underdense region, and if it does, it will result in stronger demagnification, because these regions are more underdense. In the case of magnification, these effects act in opposite directions, and almost perfectly cancel each other, making the distributions at values of $\mu > 1$ appear independent of σ_8.

https://doi.org/10.1071/AS01022 Published online by Cambridge University Press

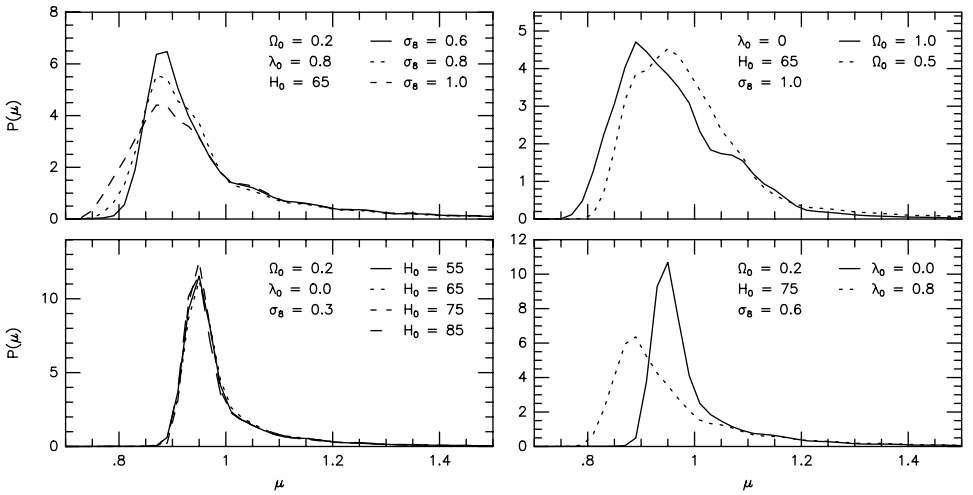

Figure 1 Magnification distributions for various models, showing the effect of varying σ_8 (top left panel), H_0 (bottom left panel), Ω_0 (top right panel), and λ_0 (bottom right panel).

The bottom left panel shows the effect of varying H_0. The distribution is independent of H_0. This results from competing effects: the cosmological distances are shorter in models with large H_0, resulting in a weaker lensing, but this effect is compensated by the fact that at fixed Ω_0, the mean background density increases like H_0^2. The top right panel shows the effect of varying Ω_0. Of all the various dependences, the Ω_0 dependence is the most difficult one to interpret as we are dealing with three concurrent effects. As Ω_0 increases, the dependence upon the mean background density yields stronger lensing effects, while the dependences upon the cosmological distances and the large-scale structure yields weaker lensing effects. The importance of lensing increases with Ω_0, resulting in a shift of the distribution toward lower values. The dominant effect in this regime is therefore the mean background density.

The bottom right panel shows the effect of varying λ_0. The presence of a cosmological constant increases the effect of magnification by increasing the cosmological distances. The cosmological constant results in a widening of the distribution, and a shift toward lower magnifications. The high magnification tail depends on the intrinsic properties of the galaxies, but not on their actual locations or level of clustering.

The *magnification probability* P_M is defined as the probability that a random source is magnified (i.e. $\mu > 1$). In Figure 2, we plot P_M vs. σ_8, for all models. P_M is essentially independent of σ_8. This could have been anticipated from Figure 1, which showed that for most models, $P(\mu)$ is independent of σ_8 for $\mu > 1$.

4.2 *The Shear Distributions*

Figure 3 shows the shear distribution $P(a_1/a_2)$ for various models, where a_1 and a_2 are the major and minor axes of the images, respectively. The top left panel shows the effect of varying σ_8. As σ_8 increases, the peak of the distribution decreases while the high-tail of the distribution increases. This was expected, since the large-scale structure, whose amplitude is measured by σ_8, is the primary origin of the shear.

The bottom left panel shows the effect of varying H_0. The curves in each panel are very similar. The absence of dependence upon H_0 results from competing effects. With larger H_0, the mean background density is higher, increasing the effects of lensing, but the cosmological distances are shorter, decreasing the effects of lensing.

The top right panel shows the effect of varying Ω_0. The dependence upon the mean background density dominates, and consequently the distribution is wider for models with larger Ω_0.

The bottom right panel shows the effect of varying λ_0. As λ_0 increases, the distributions become wider, indicating that the effect of lensing is stronger. A larger value of λ_0 results in larger cosmological distances, which is clearly the dominant effect here.

4.3 *Double Images*

For each model, we computed the probability P_2 of finding a double image. The results are plotted in Figure 4. There are 43 points in each panel, corresponding to the 43 different cosmological models considered. There is a strong trend for P_2 to increase with λ_0.

To study the variations of P_2 with the other parameters *at fixed* λ_0, we use different symbols to designate the different values of λ_0. The large scatter in the values of P_2 is clearly caused by the dependence of P_2 upon λ_0. On all panels, $\lambda_0 = 0.8$ models (solid circles) are concentrated at the top, while $\lambda_0 = 0$ models (crosses) are concentrated at the bottom. P_2 is essentially independent of Ω_0, H_0, and σ_8 at fixed λ_0. These results imply that (1) double images, and multiple images in general, are caused by galaxies and not by the background large-scale structure, and (2) the strong dependence of P_2 upon λ_0 indicates that the cosmological distances are the dominant effect in multiple imaging.

https://doi.org/10.1071/AS01022 Published online by Cambridge University Press

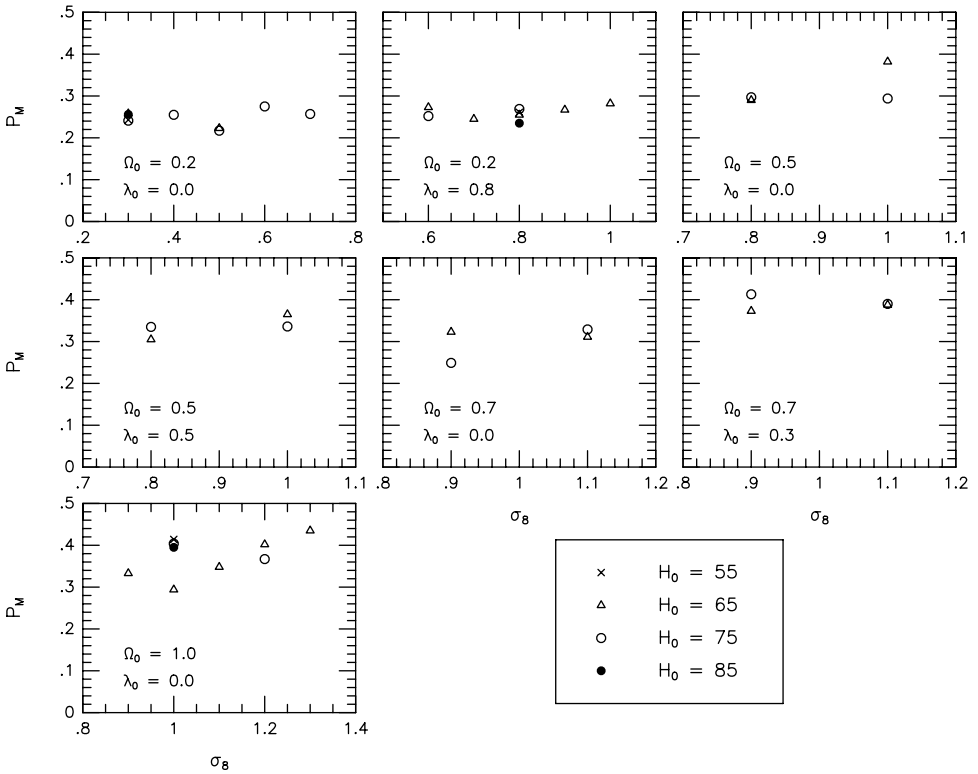

Figure 2 Magnification probability P_M vs. σ_8. The values of Ω_0 and λ_0 are indicated in each panel. The various symbols correspond to various values of H_0.

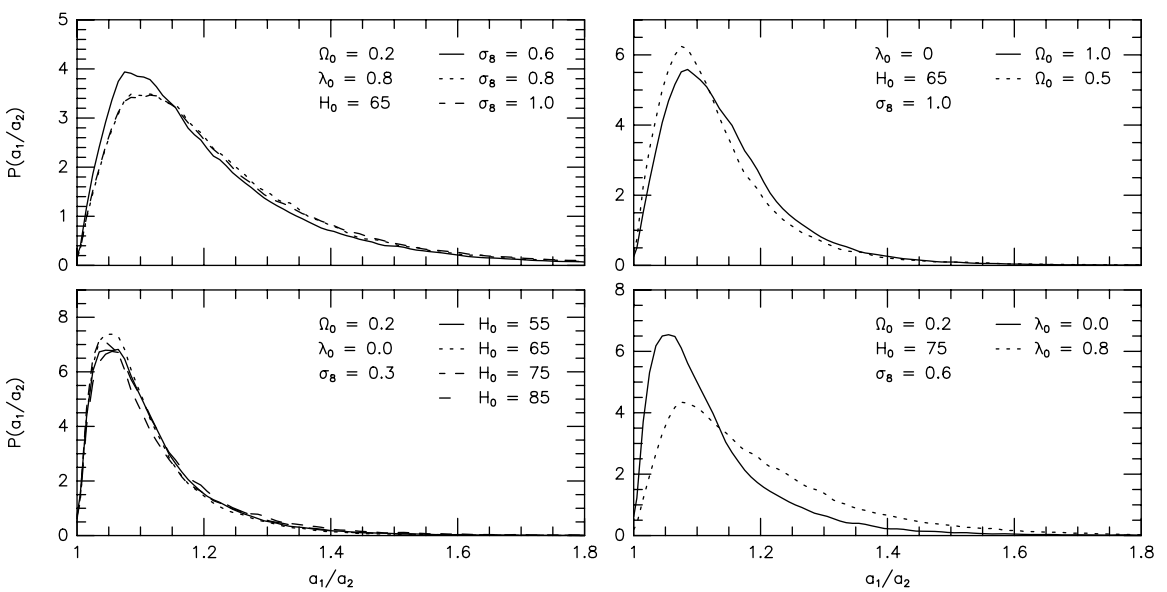

Figure 3 Shear distributions for various models, showing the effect of varying σ_8 (top left panel), H_0 (bottom left panel), Ω_0 (top right panel), and λ_0 (bottom right panel).

4.4 The Distribution of Image Separations

Figure 5 shows histograms of the angular separations (in arcseconds) of all the double image cases, for models with $\Omega_0 = 1$, $\lambda_0 = 0$, and $\Omega_0 = 0.2$, $\lambda_0 = 0.8$. Several trends are apparent. We are considering sources with an angular diameter of $1''$, hence the smallest possible image separation is of order $0.5''$. Most histograms in Figure 5 show a distribution that rises sharply from $0.5''$ to $1''$, and then drops slowly at larger separations, with a high-tail that extends to separations of order $4''$–$6''$.

As in the case of the double-image probability P_2, we find no obvious correlation between the shape of the histograms and the value of σ_8, again indicating that double images are caused primarily by individual galaxies, and

https://doi.org/10.1071/AS01022 Published online by Cambridge University Press

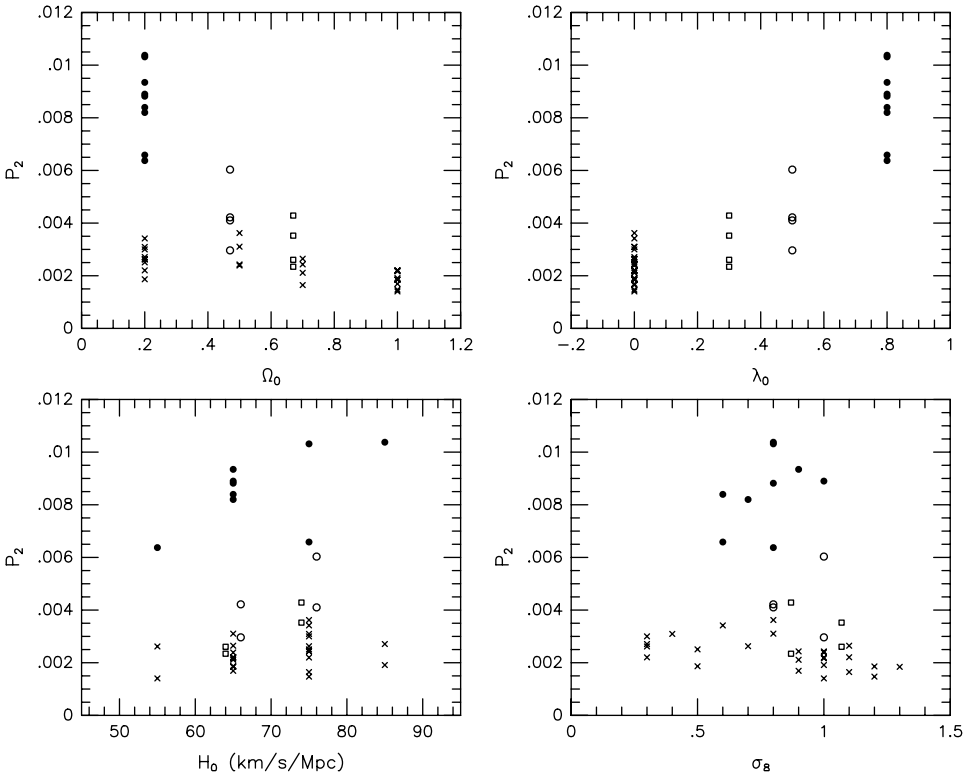

Figure 4 Double-image probability P_2, versus Ω_0 (top left panel), λ_0 (top right panel), H_0 (bottom left panel), and σ_8 (bottom right panel). Each point corresponds to one cosmological model. Symbols indicate the value of the cosmological constant; crosses: $\lambda_0 = 0$; open squares: $\lambda_0 = 0.3$; open circles: $\lambda_0 = 0.5$; filled circles: $\lambda_0 = 0.8$.

not by the large-scale structure. There is, however, a relationship between the largest angular separations and the value of λ_0. For models with $\lambda_0 = 0$, the high-tail of the distribution function rarely extends beyond $4''$, while for $\lambda_0 = 0.8$ models, the high-tail often extends to separations of $6''$. As for the probability P_2, the shape of the high-tail depends strongly upon the cosmological distances. Increasing these distances results in higher image separations for a given lensing galaxy. This affects the magnification distribution, by extending the high-tail to higher separation, and also the probability P_2, by 'separating' images that otherwise would have overlapped and been detected as a single image.

For about one of every four models, mostly the ones with $\lambda_0 > 0$, we see a secondary peak at large separation. Consider for instance the model $\Omega_0 = 0.2$, $\lambda_0 = 0.8$, $H_0 = 65\,\mathrm{km\,s^{-1}Mpc^{-1}}$, $\sigma_8 = 0.8$, which is indicated by an asterisk in Figure 5. There are no double images with separations between $4.00''$ and $4.75''$, but there are several images with separations larger that $4.75''$. This might seem like a very small effect that could be dismissed as a statistical fluctuation, but this feature is found in many histograms, suggesting that it could actually be real. This could possibly result from a coupling between galaxies and large-scale structure. Galaxies are predominantly responsible for multiple imaging. But most galaxies are located inside clusters, where the density of background matter is high. This background matter might amplify the lensing effect of the galaxy, resulting in a peak at high separation angles. This issue requires further investigation.

5 Summary

We summarise the results as follows: (1) The cosmological distances play a critical role in nearly every aspect of gravitational lensing, both weak and strong. Consequently, the properties of gravitational lenses depend much more strongly upon λ_0 than any other cosmological parameters. (2) Magnification and shear are examples of weak lensing caused primarily by the distribution of background matter, with negligible contribution from galaxies. Consequently, these effects are sensitive to the value of σ_8. (3) Multiple images are examples of strong lensing, caused mainly by galaxies. Consequently, the properties of multiple images are independent of σ_8. They are determined by the cosmological distances, which depend primarily upon λ_0, and by the details of the galactic models, which are usually independent of the cosmological parameters. Therefore, observations of weak lensing can be used to determine the cosmological constant and the *unbiased* density structure of the universe, while observations of strong lensing can be used to determine the cosmological constant and the internal structure of galaxies and clusters. (4) The dependence upon H_0 and Ω_0, is not as simple, because varying these parameters affects gravitational lensing in several ways that often partly cancel one another. Determining

https://doi.org/10.1071/AS01022 Published online by Cambridge University Press

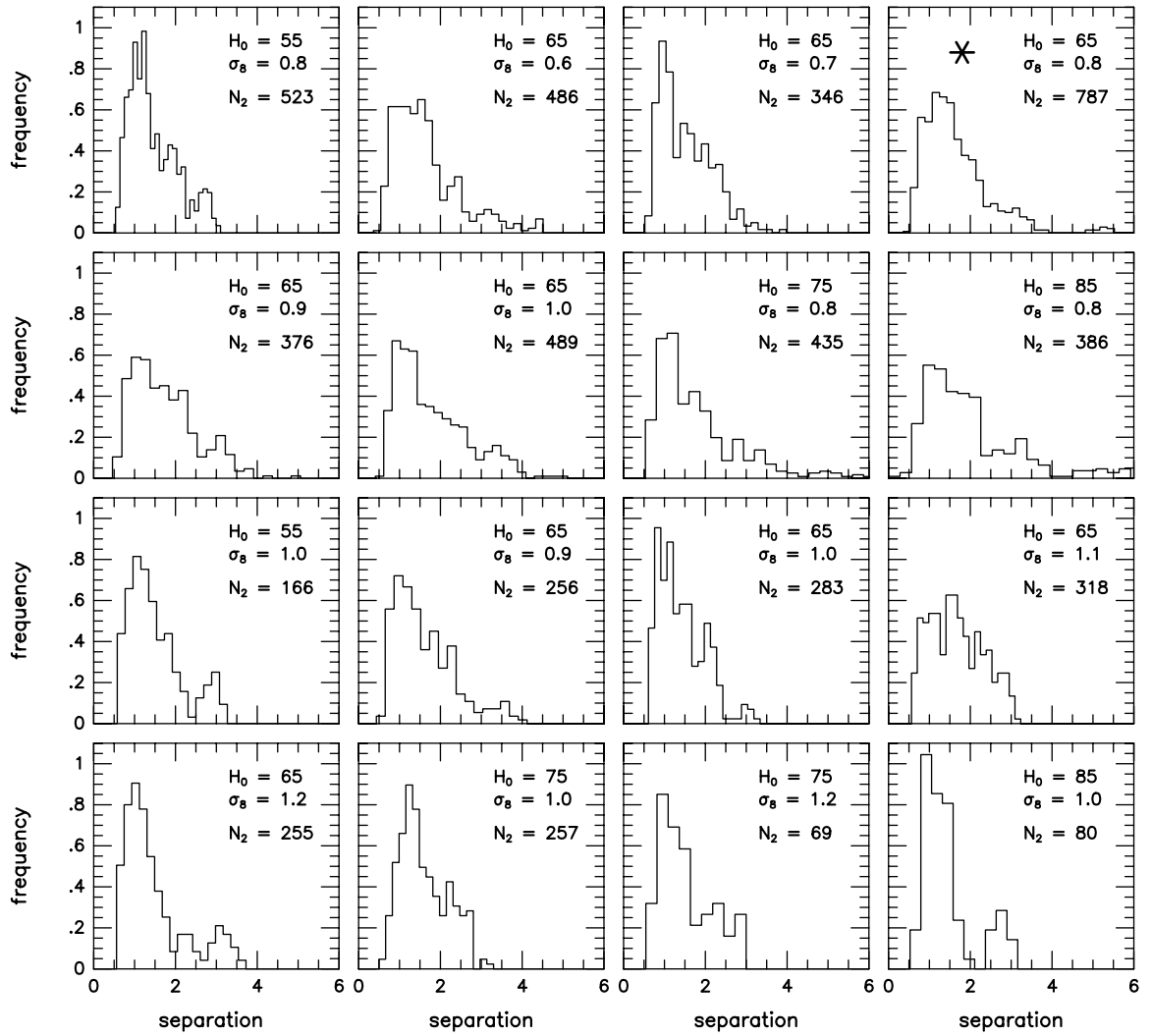

Figure 5 Histograms of the distribution of image separations in arc seconds, for various models. Top two rows: models with $\Omega_0 = 0.2$, $\lambda_0 = 0.8$; bottom two rows: models with $\Omega_0 = 1$, $\lambda_0 = 0$. The values of H_0 (in units of km s^{-1}Mpc^{-1}), σ_8, and the number of double images are indicated.

λ_0 and σ_8 from observations seems much more promising than determining Ω_0 and H_0. The complete results of this survey are described in greater detail in Premadi et al. (2001).

References

Barber, A. J., Thomas, P. A., Couchman, H. M. P., & Fluke, C. J. 2000, MNRAS, 319, 267
Chiba, M., & Yoshii, Y. 1999, ApJ, 510, 42
Falco, E. E., Kochanek, C. S., & Muñoz, J. A. 1998, ApJ, 494, 47
Fukugita, M., Futamase, T., & Kasai, M. 1990, MNRAS, 246, 24P
Jaroszyński, M. 1992, MNRAS, 255, 655
Kundić, T., et al. 1997, ApJ, 482, 75
Martel, H., Premadi, P., & Matzner, R. 1998, ApJ, 497, 512
Martínez-González, E., Sanz, J. L., & Cayón, L. 1997, ApJ, 484, 1
Premadi, P., Martel, H., & Matzner, R. 1998, ApJ, 493, 10
Premadi, P., Martel, H., Matzner, R., & Futamase, T. 2001, ApJS, in press (astro-ph/0101359)
Schneider, P., Ehlers, L., & Falco, E. E. 1992, Gravitational Lenses (Berlin: Springer-Verlag)
Turner, E. L. 1990, ApJ, 365, L43
Wambsganss, J., Cen, R., Xu, G., & Ostriker, J. P. 1997, ApJ, 475, L81

https://doi.org/10.1071/AS01022 Published online by Cambridge University Press